

## A SPECIAL FINITE ELEMENT METHOD BASED ON COMPONENT MODE SYNTHESIS

U. L. HETMANIUK<sup>1</sup> AND R. B. LEHOUCQ<sup>2</sup>

**Abstract.** The goal of our paper is to introduce basis functions for the finite element discretization of a second order linear elliptic operator with rough or highly oscillating coefficients. The proposed basis functions are inspired by the classic idea of component mode synthesis and exploit an orthogonal decomposition of the trial subspace to minimize the energy. Numerical experiments illustrate the effectiveness of the proposed basis functions.

**1991 Mathematics Subject Classification.** 35J20, 65F15, 65N25, 65N30, 65N55.

10 September 2009.

### 1. INTRODUCTION

The finite element solution of the partial differential equation

$$\begin{cases} -\nabla \cdot (c(\mathbf{x})\nabla u(\mathbf{x})) & = f(\mathbf{x}) & \text{in } \Omega, \\ u & = 0 & \text{on } \partial\Omega, \end{cases} \quad (1)$$

has been the subject of much research. Difficulties arise when the coefficient  $c$  associated with the second order linear elliptic operator is rough or highly oscillating so that a standard application of the finite element method necessitates a highly refined mesh. An important task is to define an appropriate approximation space that has knowledge of the coefficient  $c$ , followed by an adroit choice of basis functions, for example functions of local support. These functions give rise to an effective finite element method when a reasonably implemented algorithm with acceptable performance and sufficient accuracy results. Babuška, Caloz, and Osborn [3, p. 947] denote such finite element methods *special*.

The goal of our paper is to determine a conforming approximation space of functions for the finite element solution of (1). In contrast to other approaches, we exploit the fact that the solution  $u$  of (1) solves the minimization problem

$$\arg \min_{v \in H_0^1(\Omega)} \left( \frac{1}{2} \int_{\Omega} c(\mathbf{x}) |\nabla v(\mathbf{x})|^2 d\mathbf{x} - \int_{\Omega} f(\mathbf{x})v(\mathbf{x}) d\mathbf{x} \right) \quad (2)$$

and therefore is the minimum energy solution. This energy principle represents an intrinsic metric for comparing the quality of approximations to the solution of (1). Our procedure is based upon the classic idea of component

---

*Keywords and phrases:* eigenvalues, modal analysis, multilevel, substructuring, domain decomposition, dimensional reduction, finite elements

<sup>1</sup> Department of Applied Maths, University of Washington, Box 352420, Seattle, WA 98195-2420, (hetmaniu@u.washington.edu)

<sup>2</sup> Sandia National Laboratories, P.O. Box 5800, MS 1320, Albuquerque, NM 87185-1320 (rblehou@sandia.gov)

mode synthesis (CMS), introduced in [8, 12]. Starting from a partition of the domain  $\Omega$ , component mode synthesis methods exploit an orthogonal decomposition of  $H_0^1(\Omega)$  to solve the optimality system associated with (2). Motivated by this orthogonal decomposition, we develop a conforming finite dimensional approximation space. We contrast our CMS-based approach with the multiscale finite element method (MsFEM) [9] and draw a relationship with the generalized finite element method (GFEM) [2]. We argue that our approach does not fit exactly into the framework of generalized finite element methods (in contrast to MsFEM). We demonstrate the efficacy of our CMS-based approach through a suite of careful numerical experiments.

### 1.1. Notation and assumptions

We quickly review our use of standard notation. Let  $\Omega$  be a two- or three-dimensional domain with Lipschitz boundary  $\partial\Omega$  and so let  $H^1(\Omega)$  denote a Sobolev space of order 1; let  $H_0^1(\Omega)$  denote a subspace of  $H^1(\Omega)$  consisting of functions that vanish on  $\partial\Omega$ . Let the norm and inner product on  $H^1(\Omega)$  and  $L^2(\Omega)$  be given by  $\|\cdot\|_1$ ,  $(\cdot, \cdot)_1$ , and  $\|\cdot\|$ ,  $(\cdot, \cdot)$ , respectively. Let

$$a(u, v) = \int_{\Omega} c(\mathbf{x}) \nabla u(\mathbf{x}) \cdot \nabla v(\mathbf{x}) d\mathbf{x}, \quad (3)$$

denote the bilinear form induced by (1). We suppose that  $a(\cdot, \cdot)$  is coercive,

$$\exists \alpha > 0, \quad 0 < \alpha \|v\|_1^2 \leq a(v, v), \quad \forall v \in H_0^1(\Omega), \quad (4)$$

and continuous,

$$\exists \gamma > 0, \quad a(v, w) \leq \gamma \|v\|_1 \|w\|_1 \quad \forall v, w \in H_0^1(\Omega). \quad (5)$$

We rewrite (2) as

$$\arg \min_{v \in H_0^1(\Omega)} \left( \frac{1}{2} a(v, v) - (f, v) \right), \quad (6)$$

and the associated optimality system is the variational formulation of (1), e.g. given  $f \in L^2(\Omega)$ , find  $u \in H_0^1(\Omega)$  such that

$$a(u, v) = (f, v) \quad \forall v \in H_0^1(\Omega). \quad (7)$$

We refer to the solutions of (1), (2), and (7) as equivalent in a formal sense. Our approach is not restricted to (1). Other coercive and continuous bilinear forms  $a$  can be considered, such as elastostatics.

## 2. COMPONENT MODE SYNTHESIS

We review the classical technique of component mode synthesis [8, 12] from an abstract perspective. Partition the domain  $\Omega$  into  $J$  non intersecting subdomains  $\Omega_j, j = 1, \dots, J$ , that share the common interface  $\Gamma$ ; see figure 1 for the case of 4 subdomains.

Let  $V_{\Omega_j}$  be the subspace of local functions that are nonzero in  $\Omega_j$  and are trivially extended throughout  $\Omega$ ,

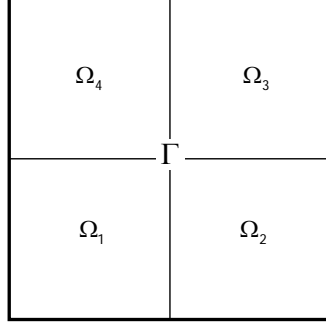
$$V_{\Omega_j} = \{v \in H_0^1(\Omega) : v|_{\Omega \setminus \Omega_j} = 0\}. \quad (8)$$

We remark that any member function of  $V_{\Omega_j}$  has a zero trace on the boundary  $\partial\Omega$  and on the interface  $\Gamma$ . Let  $V_{\Gamma}$  be the subspace of harmonic extensions of trace functions on  $\Gamma$ ,

$$V_{\Gamma} = \{E_{\Omega} \tau \in H_0^1(\Omega) : \tau \in H_0^{1/2}(\Gamma)\}, \quad (9)$$

where  $H_0^{1/2}(\Gamma)$  denotes the trace space of  $H_0^1(\Omega)$  on  $\Gamma$  and the harmonic extension  $E_{\Omega}$  of  $\tau \in H_0^{1/2}(\Gamma)$  solves the minimization problem

$$\inf_{v \in H_0^1(\Omega)} a(v, v) \quad \text{subject to} \quad v|_{\Gamma} = \tau.$$

FIGURE 1. The domain  $\Omega$  partitioned four subdomains.

We remark that the harmonic extension  $E_\Omega$  satisfies also

$$\begin{cases} -\nabla \cdot (c(\mathbf{x})\nabla E_\Omega \tau(\mathbf{x})) &= 0 & \text{in } \Omega_j, \text{ for all } j, \\ E_\Omega \tau &= \tau & \text{on } \Gamma, \\ E_\Omega \tau &= 0 & \text{on } \partial\Omega. \end{cases} \quad (10)$$

This property indicates that functions in  $V_\Gamma$  are governed by the underlying partial differential equation. Note that any non-zero member function of  $V_\Gamma$  has a non-zero trace on  $\Gamma$ . The spaces  $V_\Gamma$  and  $V_{\Omega_j}$  contain the components of the solution among, and within the subdomains, respectively, associated with a rough or highly oscillating coefficient  $c$ .

A key result is the orthogonal decomposition

$$H_0^1(\Omega) = \left( \bigoplus_{j=1}^J V_{\Omega_j} \right) \oplus V_\Gamma. \quad (11)$$

Although not often stated in this form, this is a well-known result, at the heart of the analysis and development of domain decomposition methods for elliptic partial differential equations [14], and modern component mode synthesis methods [5,6].

The decomposition (11) is orthogonal with respect to the inner product  $a(\cdot, \cdot)$  because

$$a(v_i, v_j) = 0, \quad \forall v_i \in V_{\Omega_i}, \quad \forall v_j \in V_{\Omega_j}, \quad (i \neq j), \quad (12a)$$

$$a(v_i, v_\Gamma) = 0, \quad \forall v_i \in V_{\Omega_i}, \quad \forall v_\Gamma \in V_\Gamma. \quad (12b)$$

The former equality follows because the supports of the two functions  $v_i$  and  $v_j$  are disjoint. The latter equality follows by definition of the harmonic extension (10).

The decomposition (11) also implies that

$$\min_{v \in H_0^1(\Omega)} \left( \frac{1}{2} a(v, v) - (f, v) \right) = \sum_{j=1}^J \min_{v \in V_{\Omega_j}} \left( \frac{1}{2} a(v, v) - (f, v) \right) + \min_{v \in V_\Gamma} \left( \frac{1}{2} a(v, v) - (f, v) \right). \quad (13)$$

The solution of (7) is the sum of  $J$  local functions, respectively in  $V_{\Omega_1}, \dots, V_{\Omega_J}$ , and a function of  $V_\Gamma$ , *i.e.*

$$u = u_1 + \dots + u_J + u_\Gamma, \quad (14)$$

where  $u_j$  and  $u_\Gamma$  minimizes the energy in  $V_{\Omega_j}$  and  $V_\Gamma$ , respectively. The local function  $u_j \in V_{\Omega_j}$  satisfies

$$a(u_j, v) = (f, v), \quad \forall v \in V_{\Omega_j}, \quad (15)$$

and is also the orthogonal projection of  $u$  onto  $V_{\Omega_j}$ . The function  $u_\Gamma \in V_\Gamma$  satisfies

$$a(u_\Gamma, v) = (f, v), \quad \forall v \in V_\Gamma, \quad (16)$$

and is also the orthogonal projection of  $u$  onto  $V_\Gamma$ .

The orthogonal decomposition of the solution given by (14) explains that the purpose of  $u_\Gamma \in V_\Gamma$  is to couple the  $J$  subdomain solutions  $u_j$ . Component mode synthesis is thus defined where components from the  $J + 1$  subspaces are synthesized to approximate a function over  $\Omega$ .

An approximating subspace consistent with the decomposition (11) arises from selecting a subset of eigenmodes<sup>1</sup> for  $a(\cdot, \cdot)$  in the subspaces  $V_{\Omega_j}$  and  $V_\Gamma$ . To build this approximating subspace, we introduce two different sets of eigenvalue problems. First, we define  $J$  *fixed-interface* eigenvalue problems: Find  $(z_{*,j}, \lambda_{*,j}) \in V_{\Omega_j} \times \mathbb{R}$  such that

$$a(z_{*,j}, v) = \lambda_{*,j} (z_{*,j}, v) \quad \forall v \in V_{\Omega_j}, \quad (17)$$

and, then, the *coupling* eigenvalue problem: Find  $(z_{*,\Gamma}, \lambda_{*,\Gamma}) \in V_\Gamma \times \mathbb{R}$  such that

$$a(z_{*,\Gamma}, v) = \lambda_{*,\Gamma} (z_{*,\Gamma}, v) \quad \forall v \in V_\Gamma. \quad (18)$$

Note that the only differences between these two eigenvalue problems are the approximating spaces  $V_{\Omega_j}$  and  $V_\Gamma$ . Because a member of  $V_\Gamma$  is determined by its trace on  $\Gamma$ , the coupling eigenvalue problem (18) can be equivalently expressed as follows: Find  $(\tau_*, \lambda_{*,\Gamma}) \in H_{00}^{1/2}(\Gamma) \times \mathbb{R}$  such that

$$a(E_\Omega \tau_*, E_\Omega \eta) = \lambda_{*,\Gamma} (E_\Omega \tau_*, E_\Omega \eta) \quad \forall \eta \in H_{00}^{1/2}(\Gamma). \quad (19)$$

We assume that the eigenvalues  $\{\lambda_{i,j}\}_{i=1}^\infty$  and  $\{\lambda_{i,\Gamma}\}_{i=1}^\infty$  are ordered into nondecreasing sequences and that the eigenmodes  $z_{*,j}$  and  $z_{*,\Gamma}$  are normalized for the  $L^2$  inner product.

The fixed-interface and coupling eigenmodes can then be employed to expand the source term  $f$  and the solution  $u$  of (2)

$$u = \sum_{j=1}^J \sum_{i=1}^\infty \frac{(f, z_{i,j})}{\lambda_{i,j}} z_{i,j} + \sum_{i=1}^\infty \frac{(f, z_{i,\Gamma})}{\lambda_{i,\Gamma}} z_{i,\Gamma}. \quad (20)$$

We define the finite-dimensional subspace

$$V_{CMS} = \left( \bigoplus_{j=1}^J \text{span}\{z_{i,j}; 1 \leq i \leq I_j\} \right) \oplus \text{span}\{z_{i,\Gamma}; 1 \leq i \leq I_\Gamma\}, \quad (21)$$

where  $I_j$  and  $I_\Gamma$  are non-negative integers. The approximate solution  $u_{CMS}$  satisfies

$$a(u_{CMS}, v) = (f, v), \quad \forall v \in V_{CMS}, \quad (22)$$

and is given by the truncated series

$$u_{CMS} = \sum_{j=1}^J \sum_{i=1}^{I_j} \frac{(f, z_{i,j})}{\lambda_{i,j}} z_{i,j} + \sum_{i=1}^{I_\Gamma} \frac{(f, z_{i,\Gamma})}{\lambda_{i,\Gamma}} z_{i,\Gamma}. \quad (23)$$

<sup>1</sup> The *natural* choice of eigenmodes is frequent in structural analysis and optimal, among subspaces with the same dimension, in terms of  $n$ -widths (see [1, Theorem 5.1]).

The following energy estimate easily follows

$$a(u - u_{CMS}, u - u_{CMS}) \leq \sum_{j=1}^J \frac{1}{\lambda_{I_j+1,j}} \sum_{i=I_j+1}^{\infty} (f, z_{i,j})^2 + \frac{1}{\lambda_{I_\Gamma+1,\Gamma}} \sum_{i=I_\Gamma+1}^{\infty} (f, z_{i,\Gamma})^2. \quad (24)$$

This energy estimate indicates that an accurate approximation of  $u$  is obtained when fixed-interface eigenmodes and coupling modes are combined in the approximation subspace.

When the approximation subspace  $V_{CMS}$  does not contain any fixed-interface mode (*i.e.*  $V_{CMS} \subset V_\Gamma$ ), the energy norm of the error becomes

$$a(u - u_{CMS}, u - u_{CMS}) = \sum_{j=1}^J a(u_j, u_j) + \sum_{i=I_\Gamma+1}^{\infty} \frac{(f, z_{i,\Gamma})^2}{\lambda_{i,\Gamma}}. \quad (25)$$

Unless all the local solutions  $u_j \in V_{\Omega_j}$  are zero, the error  $u - u_{CMS}$  cannot converge to zero as  $I_\Gamma \rightarrow \infty$ . The components  $u_j$  satisfy also

$$a(u_j, u_j) = \int_{\Omega_j} f u_j \leq \|f\|_{L^2(\Omega_j)} \|u_j\|_{L^2(\Omega_j)} \leq C \text{diam}(\Omega_j) \|f\|_{L^2(\Omega_j)} \|\nabla u_j\|_{L^2(\Omega_j)}, \quad (26)$$

where we used the Cauchy-Schwarz and the Poincaré inequalities in succession. Coercivity (4) of the bilinear form  $a(\cdot, \cdot)$  then results in

$$a(u_j, u_j) \leq \frac{C}{\alpha} \text{diam}^2(\Omega_j) \|f\|_{L^2(\Omega_j)}^2. \quad (27)$$

When the components  $u_j$  are non-zero on a partition  $\mathcal{T}$ , the functions  $u_j$  may not be negligible. But, when the partition is refined, the subdomains  $\Omega_j$  and their diameters,  $\text{diam}(\Omega_j)$ , both decrease. So the error  $u - u_{CMS}$  can converge to zero with  $V_{CMS} \subset V_\Gamma$  as the partition is refined.

On the other hand, when the approximation subspace  $V_{CMS}$  does not contain any coupling modes (*i.e.*  $V_{CMS} \cap V_\Gamma = \{0\}$ ), the energy norm of the error becomes

$$a(u - u_{CMS}, u - u_{CMS}) = \sum_{j=1}^J \sum_{i=I_j+1}^{\infty} \frac{(f, z_{i,j})^2}{\lambda_{I_j+1,j}} + a(u_\Gamma, u_\Gamma). \quad (28)$$

Unless the coupling function  $u_\Gamma$  is zero (or the trace of  $u$  on  $\Gamma$  is zero), the error  $u - u_{CMS}$  cannot converge to zero when all the indices  $I_j$  go to infinity. Contrary to the previous case, refining the partition would make the interface  $\Gamma$  larger and so would not decrease  $a(u_\Gamma, u_\Gamma)$ .

Consequently, combining (or synthesizing) functions from both  $V_{\Omega_j}$  and  $V_\Gamma$  into the approximation subspace  $V_{CMS}$  is a strategy that can lead to an accurate approximation of  $u$  on a coarse partition  $\mathcal{T}$ .

### 3. NEW SPECIAL FINITE ELEMENT METHOD

Motivated by the orthogonal decomposition (11), our goal is to determine a finite-dimensional subspace  $V_{ACMS}$  of  $H_0^1(\Omega)$  spanned by basis functions of local support and that approximates  $V_{CMS}$  (21). The eigenmodes in  $V_{\Omega_j}$  have, by construction, local support but the coupling modes in  $V_\Gamma$  have typically global support in  $\Omega$ . So we propose to select basis functions of local support from the subspaces  $V_{\Omega_j}$  and  $V_\Gamma$ .

To simplify the presentation, we assume that  $\Omega = (0, 1) \times (0, 1)$  and that  $\mathcal{T}$  is a partition of  $\Omega$  into rectangles  $\Omega_j$ . The interface  $\Gamma$  is the union of all the interior edges between two rectangles. We remind the reader that the subspace  $V_{\Omega_j}$ , defined by (8), contain functions of zero trace on  $\Gamma$  and can only hold information on the subdomain  $\Omega_j$ . Functions of  $V_\Gamma$  (9) are governed by the underlying partial differential equation because they are harmonic extensions in  $\Omega$  of trace functions on  $\Gamma$ . They satisfy the boundary value problem (10).

The conforming discretization space we propose is consistent with the decomposition (11) and the basis functions have local support. With the partition  $\mathcal{T}$ , we define the subspace

$$V_{ACMS} := \left( \bigoplus_{j=1}^J \text{span}\{z_{1,j}\} \right) \oplus \left[ \left( \bigoplus_{P \in \Omega} \text{span}\{\varphi_P\} \right) \oplus \left( \bigoplus_{e \subset \Omega} \text{span}\{\psi_e\} \right) \right], \quad (29)$$

where  $z_{1,j}$  is the first *fixed-interface* mode (17) in  $\Omega_j$  and the letter  $A$  in  $ACMS$  stands for approximate. Note that the vertices  $P$  and the edges  $e$  are taken in the interior of  $\Omega$ . The Dirichlet boundary condition is built into  $V_{ACMS}$ .

For any interior point  $P$  of the partition  $\mathcal{T}$ ,  $\varphi_P$  belongs to  $V_\Gamma$  and is a harmonic extension satisfying

$$\begin{cases} -\nabla \cdot (c(\mathbf{x})\nabla \varphi_P(\mathbf{x})) = 0 & \text{in } \Omega_j, \\ \varphi_P = 0 & \text{on } \partial\Omega, \\ \varphi_P \neq 0 & \text{on } \Gamma, \\ \varphi_P(P') = \delta_{P,P'} & \end{cases} \quad (30)$$

for any element  $\Omega_j$ , where  $\delta_{P,P'}$  is the Kronecker delta function. On  $\Gamma$ , we select a trace for  $\varphi_P$  that has local support along the boundaries of elements sharing the vertex  $P$ . The resulting function  $\varphi_P$  will also have as support the elements sharing the point  $P$ . On a horizontal edge  $[x_L, x_P] \times \{y_P\}$ , the trace for  $\varphi_P$  is defined by

$$\varphi_P(x, y_P) = \left( \int_{x_L}^x \frac{ds}{c(s, y_P)} \right) / \left( \int_{x_L}^{x_P} \frac{ds}{c(s, y_P)} \right) \quad \forall x \in [x_L, x_P]. \quad (31)$$

Along a vertical edge, a similar definition is used.<sup>2</sup> Figure 2 plots an example of trace for  $\varphi_P$ . Note that the

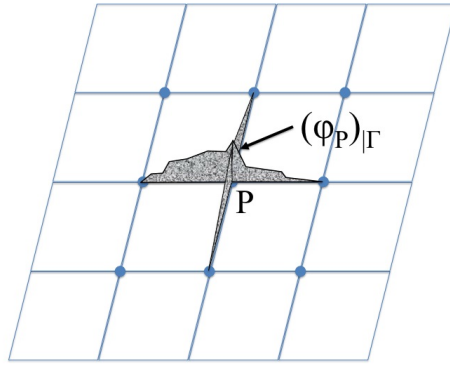


FIGURE 2. Trace of  $\varphi_P$  along  $\Gamma$  for a domain partitioned into 16 subdomains

trace is piecewise monotonic along the edges.

The function  $\psi_e$ , where  $e$  is an interior edge, belongs also to  $V_\Gamma$  and is the harmonic extension of  $\tau_e \in H_{00}^{1/2}(\Gamma)$ , whose support is the edge,  $e$ , between two elements. The trace function  $\tau_e$  is the first eigenmode for the *coupling* mode problem:

$$a(E_\Omega \tau_e, E_\Omega \eta) = \lambda(E_\Omega \tau_e, E_\Omega \eta), \quad \forall \eta \in H_{00}^{1/2}(\Gamma) \text{ such that } \text{supp}(\eta) \subset e. \quad (32)$$

An example for  $\tau_e = (\psi_e)|_\Gamma$  is given in figure 3. The function  $\psi_e$  satisfies also

<sup>2</sup> Hou and Wu [11, Section 2.2] proposed the two-dimensional trace (31) in their MsFEM-O approach. This trace is motivated by one-dimensional problems for which Babuška and Osborn [4] recommended the local approximation,  $\text{span}\left\{1, \int_{x_0}^x \frac{ds}{c(s)}\right\}$  instead of  $\text{span}\{1, x\}$ .

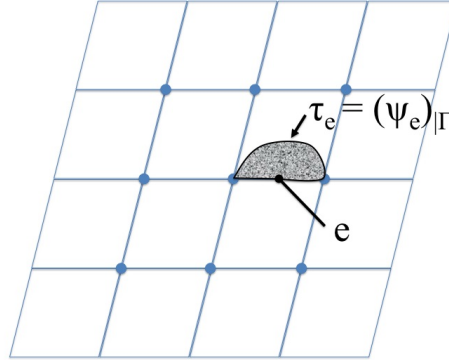


FIGURE 3. Example of a local coupling mode along an interior edge  $e$ .

$$\begin{cases} -\nabla \cdot (c(\mathbf{x}) \nabla \psi_e(\mathbf{x})) &= \lambda \psi_e & \text{in } \Omega_j, \\ \psi_e &= 0 & \text{on } \partial\Omega, \\ \psi_e &= \tau_e & \text{on } \Gamma, \end{cases} \quad (33)$$

for any element  $\Omega_j$ .

In summary, the conforming finite-dimensional subspace  $V_{ACMS} \subset H_0^1(\Omega)$  exploits the orthogonal decomposition (11) for incorporating information on the variational form  $a(\cdot, \cdot)$ . The subspace  $V_{ACMS}$  contains information within subdomains  $\Omega_j$  via the first fixed-interface mode. The functions  $\varphi_P$  and  $\psi_e$  carry information among four and two subdomains, respectively. These three special basis functions have local support. The generalization of  $V_{ACMS}$  to triangular cells is straightforward.

The special basis functions  $z_{1,j}$ ,  $\varphi_P$ , and  $\psi_e$  are obtained numerically. They are computed via a finite element discretization within each element  $\Omega_j$ . Local problems are solved to obtain the functions  $z_{1,j}$ ,  $\varphi_P$ , and  $\psi_e$  (which can be done in parallel). In a second step, a global problem is solved to compute the approximate solution  $u_{ACMS}$  in  $V_{ACMS}$ . Further details are given in section 5. Before presenting the numerical experiments, we discuss other choices of finite-dimensional approximation subspaces.

**Remark 1.** *By introducing subdomains, the cost of computing eigenmodes in  $V_{\Omega_j}$  is tractable. However, computing the coupling eigenmodes (19) associated with  $V_{CMS}$  is nontrivial because a generalized eigenvalue problem composed of Schur and mass complement operators represents a significant computation; see the survey paper [10] for details.*

#### 4. RELATIONSHIP TO OTHER APPROXIMATING METHODS

Numerous choices of basis functions are possible for defining a finite dimensional subspace of  $H_0^1(\Omega)$ . Babuška, Caloz, and Osborn [3] use the phrase *special finite elements* to denote finite element methods (FEM) that employ basis functions that, for instance, incorporate specialized knowledge of the partial differential operator. Many methods have been proposed to incorporate relevant information into the special basis functions; for instance the generalized FEM (GFEM) [2] and the multiscale FEM (MsFEM) [9]. The purpose of this section is to compare the special finite element introduced in section 3 for the solution of (1) with the classical FEM, MsFEM, and GFEM. We only consider comparisons with conforming finite element methods and with methods that do not lead to modifications of the variational formulation, e.g. the bilinear and linear forms of (7) are not modified. For instance, MsFEM with oversampling is a nonconforming finite element method [9, p.23] and the recent multiscale framework presented by Nolen, Papanicolaou and Pironneau [13] modifies the variational formulation.

#### 4.1. Classical FEM

The standard nodal linear finite element method (Q1) defines an approximation subspace  $V_{Q1}$

$$V_{Q1} := \text{span} \{N_P; P \in \mathcal{T}\}, \quad (34)$$

where  $N_P$  is the bilinear nodal shape function for an interior point  $P$ . When  $c$  is a constant, for any interior point  $P$ , the associated nodal shape function  $N_P$  belongs to  $V_\Gamma$  because  $N_P$  satisfies

$$\begin{cases} -\Delta N_P = 0 & \text{in } \Omega_j, \text{ for all } j, \\ N_P \neq 0 & \text{on } \Gamma, \\ N_P = 0 & \text{on } \partial\Omega. \end{cases} \quad (35)$$

Therefore  $V_{Q1}$  is a finite-dimensional subspace of  $V_\Gamma$  that is orthogonal to the subspaces  $V_{\Omega_j}$ .

However, when  $c$  is not equal to a constant, the approximation subspace  $V_{Q1}$  is no longer a subspace of  $V_\Gamma$ . For any interior point  $P$ , the nodal shape function  $N_P$  is not a member of  $V_\Gamma$  because  $N_P$  is no longer an harmonic extension, *i.e.*

$$\nabla \cdot (c(\mathbf{x}) \nabla N_P(\mathbf{x})) \neq 0 \quad \text{in } \Omega_j, \quad (36)$$

when  $\Omega_j$  intersects the support of  $N_P$ . The nodal shape function  $N_P$  is not a member of  $\Omega_j$  either because its trace on  $\Gamma$  is non zero. Therefore the nodal shape function  $N_P$  has nonzero components in  $V_\Gamma$  and some  $V_{\Omega_j}$  in stark contrast to  $\varphi_P$  defined by (30).

#### 4.2. MsFEM

The MsFEM of Hou and Wu [11] selects basis functions exclusively from  $V_\Gamma$ . A MsFEM basis function  $\varphi_P$  is defined by (30) and its trace along the interface  $\Gamma$ . This choice leads to the approximating subspace

$$V_{MsFEM} := \bigoplus_{P \in \Omega} \text{span}\{\varphi_P\} \subset V_\Gamma \subset H_0^1(\Omega), \quad (37)$$

When  $c$  is constant, the MsFEM is equivalent to the linear finite element method, e.g.,  $V_{MsFEM} = V_{Q1}$ . When  $c$  is not equal to a constant,  $V_{MsFEM}$  is no longer equal to  $V_{Q1}$  but remains a subspace of  $V_\Gamma$ . The orthogonal decomposition (11) indicates that MsFEM is a generalization of the linear finite element method for a nonconstant coefficient  $c$  because  $V_{MsFEM} \subset V_\Gamma$ . When the partition  $\mathcal{T}$  is coarse, components in  $V_{\Omega_j}$  of the solution  $u$  are not computed by  $V_{MsFEM}$  and this error may limit the accuracy of the computed solution in  $V_{MsFEM}$ . This limitation is also explained by the error analysis (25)–(27) that results from the absence of components in  $V_{\Omega_j}$ . To remove this limitation and decrease the error, a partition finer than  $\mathcal{T}$  needs to be used.

The MsFEM-O<sup>3</sup> arises when  $\varphi_P$  is the same harmonic extension used in  $V_{ACMS}$ , defined by (30) and the trace (31). On the other hand, the MsFEM-L results when the trace of  $\varphi_P$  on  $\Gamma$  is set equal to the trace of  $N_P$ . In an attempt to mitigate the resonance effect that arises when using MsFEM-L and MsFEM-O, MsFEM-os-L introduces oversampling; see Efendiev and Hou [11, Section 2.3] for a discussion. However, oversampling leads to discontinuous basis functions and, hence, a nonconforming finite element method. In contrast, the method proposed in section 3 is conforming.

#### 4.3. GFEM

The GFEM space is formally defined by

$$V_{GFEM} := \left\{ \sum_{j=1}^N \phi_j \xi_j : \xi_j \in S_j, \quad \sum_{j=1}^N \phi_j = 1 \text{ on } \Omega, \quad \Omega = \bigcup_j \omega_j, \quad \phi_j = 0 \text{ on } \Omega \setminus \omega_j, \quad j = 1, \dots, N \right\},$$

<sup>3</sup>Hou and Wu points that O indicates the oscillatory boundary condition defining  $\varphi_P$ . However,  $\varphi_P$  is not oscillatory because its trace is monotonic on each edge. This monotonicity arises because the coercivity of  $a$  implies that the coefficient  $c$  is positive.

where the patches  $\omega_1, \dots, \omega_N$  are open sets. The finite dimensional space  $S_j$  contains functions  $\xi_j$  defined on  $\omega_j$ ,

$$S_j = \text{span} \{ \xi_{i,j} \in H^1(\omega_j); \xi_{i,j} = 0 \text{ on } \bar{\omega}_j \cap \partial\Omega \}, \quad (38)$$

such that the functions  $\xi_j$  approximate well, on  $\omega_j$ , the solution  $u$  with respect to the energy norm. The functions  $\{\phi_j\}$  form a *partition of unity* on  $\Omega$ . Their role is to paste together the local approximation functions,  $\xi_j \in S_j$ , to form global approximation functions that are conforming, *i.e.*  $\phi_j \xi_j$  will belong to  $H_0^1(\Omega)$ . If, in addition, the functions  $\phi_j$  and their gradients  $\nabla \phi_j$  are uniformly bounded, Babuška, Banerjee, and Osborn [2] prove convergence estimates for GFEM. Note that their proof can give suboptimal convergence rates (see [2, p. 88-89]). In order to show that a special finite element method is a GFEM, we need to exhibit patches  $\{\omega_j\}$ , the partition of unity  $\{\phi_j\}$ , and subspaces  $S_1, \dots, S_N$ .

We now establish a relationship between  $V_{ACMS}$  and  $V_{GFEM}$  in two steps. We first demonstrate that MsFEM is a generalized finite element method<sup>4</sup>. Second, we show that  $V_{ACMS}$  is a proper subspace of a GFEM subspace.

Consider the functions  $\varphi_P$  defined by (30). The definition extends easily to the case where the vertex  $P$  belongs to  $\partial\Omega$ . Based on the choice of trace function (31), the functions  $\{\varphi_P\}$  satisfy

$$\sum_{P \in \bar{\Omega}} \varphi_P(\mathbf{x}) = 1, \quad \forall \mathbf{x} \in \Omega$$

(see also Hou and Wu [11, p. 173]). Therefore, the shape functions  $\{\varphi_P\}$  form a partition of unity on  $\Omega$ . We can select the family  $\{\phi_j\}$  to be the family  $\{\varphi_P\}$  and the patches  $\{\omega_j\}$  to be the support of the shape functions  $\varphi_P$ . Introduce the finite dimensional subspace  $S_j$ ,

$$S_j = \begin{cases} \{0\} & \text{when } \bar{\omega}_j \cap \partial\Omega \neq \emptyset, \\ \text{span}\{1\} & \text{otherwise.} \end{cases} \quad (39)$$

The space  $S_{MsFEM}$ ,

$$S_{MsFEM} = \text{span} \{ \phi_j \xi_j; \text{ where } \xi_j \in S_j \text{ defined by (39), } j = 1, \dots, N \},$$

is a generalized finite element approximation space. By construction, this space is equal to  $V_{MsFEM}$ , defined by (37). So MsFEM is a generalized finite element method where the local approximation functions  $\xi_j$  are constant and where the partition of unity functions  $\phi_j$  are harmonic extensions. This particular choice of partition of unity is unusual because the partition of unity involves the partial differential equation.

Next, for the space  $V_{ACMS}$ , the partition of unity  $\{\varphi_P\}$  and the patches  $\{\omega_j\}$  are retained. Introduce the local approximating subspace  $S_j$ ,

$$S_j = \begin{cases} \{0\} \oplus \text{span}\{\psi_e; e \subset \bar{\omega}_j \cap \Omega\} \oplus \text{span}\{z_{1,k}; \Omega_k \subset \omega_j\} & \text{when } \bar{\omega}_j \cap \partial\Omega \neq \emptyset, \\ \text{span}\{1\} \oplus \text{span}\{\psi_e; e \subset \bar{\omega}_j\} \oplus \text{span}\{z_{1,k}; \Omega_k \subset \omega_j\} & \text{otherwise.} \end{cases} \quad (40)$$

The space  $S_{ACMS}$ ,

$$S_{ACMS} = \text{span} \{ \phi_j \xi_j; \text{ where } \xi_j \in S_j \text{ defined by (40), } j = 1, \dots, N \},$$

is a generalized finite element approximation space where the local approximation functions are the constant, the edge-based functions  $\psi_e$ , and the fixed-interface modes  $z_{1,*}$ .  $V_{ACMS}$  is a subspace of  $S_{ACMS}$  because the partition of unity property implies

$$z_{1,k} = \sum_{P \in \bar{\Omega}_k} \varphi_P z_{1,k} \quad \text{and} \quad \psi_e = \sum_{P \in \bar{\Omega}_k; e \cap \bar{\Omega}_k \neq \emptyset} \varphi_P \psi_e. \quad (41)$$

<sup>4</sup>To the best of our knowledge, this relation between MsFEM and GFEM is new.

However,  $V_{ACMS}$  is different from  $S_{ACMS}$  because the dimension of  $S_{ACMS}$  is larger than the dimension of  $V_{ACMS}$ . For example, in  $S_{ACMS}$ , the functions  $\{\varphi_P z_{1,1}\}_{P \in \overline{\Omega}_1}$  are linearly independent while the definition for  $V_{ACMS}$  contains only one instance of  $z_{1,1}$ . Our proposed special finite element method is a proper subspace of  $S_{ACMS}$  and does not appear to be equivalent to a generalized finite element method. Consequently, the GFEM theory does not apply directly to  $V_{ACMS}$  (in contrast to MsFEM). Note that because the functions  $\psi_e$  and  $z_{1,*}$  belong to  $H_0^1(\Omega)$  by construction,  $V_{ACMS}$  does not require any pasting for these functions.

## 5. NUMERICAL EXPERIMENTS

We present a series of numerical experiments using our CMS-inspired special finite element method introduced in section (3). We first discuss aspects associated with the computations. The first set of experiments is on the Laplace equation. The second and third sets of experiments are on (1) with a nontrivial coefficient  $c$ . All three cases compare the proposed special FEM with MsFEM and with CMS. The second set of experiments also illustrates the effect of the fixed interface modes and of the trace functions defining  $\varphi_P$ .

### 5.1. Practical remarks

In this section, we discuss practical aspects for the numerical experiments. First we give details on obtaining the basis functions  $z_{1,*}$ ,  $\varphi_P$ , and  $\psi_e$  and on assembling the resulting stiffness matrix. We describe the sparsity of the stiffness matrix. Finally, we describe how the approximate solutions are compared.

#### 5.1.1. Computation of basis functions

Let  $\mathcal{T}_n$  be a partition of  $\Omega = (0, 1) \times (0, 1)$  with  $n$  square elements per direction and a uniform mesh size  $h = 1/n$ . To compute the special shape functions  $z_{1,*}$ ,  $\varphi_P$ , and  $\psi_e$ , each element is divided into  $m \times m$  square elements with  $h_f = h/m$ . The local submeshes are conforming among elements.

We use piecewise bilinear elements to compute the special shape functions by solving local problems. For the functions  $\varphi_P$ , we solve approximately the problem (30). This solution is local to an element  $\Omega_j$  and the corresponding linear system is of dimension  $(m-1)^2$ . For the fixed-interface modes  $z_{1,j}$ , we solve approximately (17). The corresponding discrete eigenproblem is local to  $\Omega_j$  and of dimension  $(m-1)^2$ . The first eigenmode is computed with a *direct* solver. For an edge-based function  $\psi_e$ , we solve approximately (32). Recall that, for any function  $\eta$  supported on an edge  $e$  between the elements  $\Omega_1$  and  $\Omega_2$ , its harmonic extension  $E_\Omega \eta$  has support in  $\overline{\Omega}_1 \cup \overline{\Omega}_2$ , and has the discrete representation

$$\mathbf{E}\eta = \begin{bmatrix} -\mathbf{K}_{11}^{-1}\mathbf{K}_{1e} \\ -\mathbf{K}_{22}^{-1}\mathbf{K}_{2e} \\ \mathbf{I} \end{bmatrix} \eta,$$

where  $\eta$  is the discrete representation of  $\eta$ .  $\mathbf{K}_{11}$  and  $\mathbf{K}_{22}$  are the local stiffness matrices in, respectively,  $\Omega_1$  and  $\Omega_2$ . Then we compute the first eigenmode for the pencil

$$\left( \begin{bmatrix} -\mathbf{K}_{11}^{-1}\mathbf{K}_{1e} \\ -\mathbf{K}_{22}^{-1}\mathbf{K}_{2e} \\ \mathbf{I} \end{bmatrix}^T \begin{bmatrix} \mathbf{K}_{11} & \mathbf{0} & \mathbf{K}_{1e} \\ \mathbf{0} & \mathbf{K}_{22} & \mathbf{K}_{2e} \\ \mathbf{K}_{1e}^T & \mathbf{K}_{2e}^T & \mathbf{K}_{ee} \end{bmatrix} \begin{bmatrix} -\mathbf{K}_{11}^{-1}\mathbf{K}_{1e} \\ -\mathbf{K}_{22}^{-1}\mathbf{K}_{2e} \\ \mathbf{I} \end{bmatrix}, \right. \\ \left. \begin{bmatrix} -\mathbf{K}_{11}^{-1}\mathbf{K}_{1e} \\ -\mathbf{K}_{22}^{-1}\mathbf{K}_{2e} \\ \mathbf{I} \end{bmatrix}^T \begin{bmatrix} \mathbf{M}_{11} & \mathbf{0} & \mathbf{M}_{1e} \\ \mathbf{0} & \mathbf{M}_{22} & \mathbf{M}_{2e} \\ \mathbf{M}_{1e}^T & \mathbf{M}_{2e}^T & \mathbf{M}_{ee} \end{bmatrix} \begin{bmatrix} -\mathbf{K}_{11}^{-1}\mathbf{K}_{1e} \\ -\mathbf{K}_{22}^{-1}\mathbf{K}_{2e} \\ \mathbf{I} \end{bmatrix} \right)$$

or, equivalently, the pencil of the Schur and mass complements (of dimension  $m-1$ ).

The assembly of the global stiffness matrix and the right-hand side vector requires the computation of the volume integrals, for example,

$$\int_{\Omega_1} c(\mathbf{x}) \nabla \varphi_P(\mathbf{x}) \cdot \nabla \psi_e(\mathbf{x}) d\mathbf{x}, \quad (42)$$

on  $\mathcal{T}_h$ . We exploit the expression of  $\varphi_P$  and  $\psi_e$  on the submesh contained in  $\bar{\Omega}_1$

$$\varphi_P = \sum_{P_f \in \bar{\Omega}_1} \chi_{P_f} N_{P_f} \quad \text{and} \quad \psi_e = \sum_{P_f \in \bar{\Omega}_1} \xi_{P_f} N_{P_f} \quad (43)$$

where  $N_{P_f}$  is the piecewise bilinear shape function for the point  $P_f$  on the submesh contained in  $\bar{\Omega}_1$ . Using the stiffness matrix  $\mathbf{K}_f$  computed on the submesh, we write

$$\int_{\Omega_1} c(\mathbf{x}) \nabla \varphi_P(\mathbf{x}) \cdot \nabla \psi_e(\mathbf{x}) d\mathbf{x} = \left[ (\chi_{P_f})_{P_f \in \bar{\Omega}_1} \right]^T \mathbf{K}_f \left[ (\xi_{P_f})_{P_f \in \bar{\Omega}_1} \right] \quad (44)$$

The other volume integrals are computed similarly.

### 5.1.2. Sparsity of stiffness matrix

The approximate solution to (7) in a finite-dimensional subspace will be obtained by solving a linear system with a direct solver. Table 1 lists information about the linear system for the different approximation subspaces. With bilinear finite elements, the subspace  $V_{Q1}$  has  $(n-1)^2$  degrees of freedom and, asymptotically, 9 non-zero

Subspace	Matrix Dimension	Matrix Non-Zeros
$V_{Q1}$	$(n-1)^2$	$\approx 9(n-1)^2$
$V_{MsFEM-O}$	$(n-1)^2$	$\approx 9(n-1)^2$
$V_{ACMS}$	$(2n-1)^2$	$\approx 12(2n-1)^2$
$V_{CMS}$	$(2n-1)^2$	$= (2n-1)^2$

TABLE 1. Matrix dimensions and non-zeros for different special finite element methods

entries per row. The subspace  $V_{MsFEM-O}$  generates a matrix with the same dimension and the same sparsity pattern. For our proposed special finite element method, the subspace  $V_{ACMS}$  (29) has  $n^2$  fixed interface modes,  $(n-1)^2$  functions  $\varphi_P$ , and  $2n(n-1)$  edge functions. The dimension of  $V_{ACMS}$  is

$$n^2 + (n-1)^2 + 2n(n-1) = (n+n-1)^2 = (2n-1)^2.$$

With  $V_{ACMS}$ , the stiffness matrix contains a diagonal block for the  $n^2$  fixed interface modes. A row associated with  $\varphi_P$  (respectively  $\psi_e$ ) has at most 21 (resp. 13) non-zero entries. So an estimate for the number of non-zeros is

$$1 \times n^2 + 21 \times (n-1)^2 + 13 \times 2n(n-1) \approx \left( \frac{1}{4} + \frac{21}{4} + \frac{26}{4} \right) \times (2n-1)^2 = 12 \times (2n-1)^2.$$

For the sake of comparison, we use also the subspace  $V_{CMS}$  (21) with 1 fixed-interface mode per element and  $(2n-1)^2 - n^2$  coupling modes. The dimension of  $V_{CMS}$  is also  $(2n-1)^2$ . The resulting linear system will be diagonal. We emphasize that  $V_{CMS}$  is not practical because it demands a large number of global coupling eigenmodes whose computations are daunting. However, for the numerical experiments, we will compute these global coupling eigenmodes accurately as a basis for comparison.

### 5.1.3. Metric for comparing approximate solutions

Recall that the solution  $u$  solves the minimization problem (2) and therefore is the minimum energy solution. The energy,

$$\mathcal{E}(v) = \frac{1}{2} \int_{\Omega} c(\mathbf{x}) |\nabla v(\mathbf{x})|^2 d\mathbf{x} - \int_{\Omega} f(\mathbf{x}) v(\mathbf{x}) d\mathbf{x} = \frac{1}{2} a(v, v) - (f, v),$$

represents an intrinsic metric for comparing the quality of approximations to the solution  $u$ . Between two approximate solutions, the one with lowest energy is the most accurate one.

Computing the difference between the energy of the computed solution and the energy of the exact solution  $u$  is equivalent to computing the norm of the error for the inner product  $a(\cdot, \cdot)$ . Indeed, we have

$$\begin{aligned} \left( \frac{1}{2} a(u_{Q1}, u_{Q1}) - (f, u_{Q1}) \right) - \left( \frac{1}{2} a(u, u) - (f, u) \right) &= \frac{1}{2} a(u_{Q1}, u_{Q1}) - (f, u_{Q1}) + \frac{1}{2} a(u, u) \\ &= \frac{1}{2} (a(u_{Q1}, u_{Q1}) - 2(f, u_{Q1}) + a(u, u)) \\ &= \frac{a(u - u_{Q1}, u - u_{Q1})}{2} \end{aligned}$$

when  $u_{Q1}$  is the approximate solution computed on  $V_{Q1}$  and where we used

$$a(u, u_{Q1}) = (f, u_{Q1}) \quad \text{and} \quad a(u, u) = (f, u)$$

(from (7)). This difference of energies is an intrinsic metric for comparing the quality of approximations. When the exact solution  $u$  is not explicitly known, approximating the minimal energy,

$$\mathcal{E}^* = \frac{1}{2} a(u, u) - (f, u) = -\frac{a(u, u)}{2} = -\frac{(f, u)}{2}, \quad (45)$$

is simpler than extrapolating the exact solution. In the numerical experiments, we compute the energy differences.

## 5.2. Experiments with the Laplace equation

Consider the problem

$$\begin{cases} -\Delta u &= f & \text{on } \Omega \\ u &= 0 & \text{in } \partial\Omega \end{cases} \quad (46)$$

We choose  $f(x, y) = 2x(1-x) + 2y(1-y)$  such that the exact solution  $u$  is  $x(1-x)y(1-y)$ .

Introduce a mesh  $\mathcal{T}_n$  composed of squares with uniform mesh size  $h = 1/n$ .  $\mathcal{T}_n$  contains  $n^2$  elements,  $(n-1)^2$  interior points, and  $2n(n-1)$  interior edges. We compare the accuracy of computed solutions when using different finite-dimensional subspaces.

Figure 4 plots convergence curves for the difference of energies, which is proportional to the  $H^1$  semi-norm of the error, in terms of the number of degrees of freedom. The number of degrees of freedom is, indeed, more relevant than the mesh size  $h$  or the number of elements per direction  $n$ . As highlighted in Table 1, the considered approximation subspaces have different dimensions on the same mesh  $\mathcal{T}_n$ . As expected, the bilinear finite element has a convergence rate proportional to  $h$  or inversely proportional to the square root of the total number of degrees of freedom. The curves for  $V_{CMS}$  and  $V_{ACMS}$  are indistinguishable, indicating that the basis functions in  $V_{ACMS} \cap V_{\Gamma}$  with local support approximate well the subspace spanned by the global eigenmodes for the Schur and mass complements.

For a fixed number of degrees of freedom, the approximate solutions computed in the subspaces  $V_{CMS}$  and  $V_{ACMS}$  are more accurate than in the subspace  $V_{Q1}$ . To reach a fixed level of accuracy for this problem,  $V_{CMS}$  and  $V_{ACMS}$  require 5 times less degrees of freedom than  $V_{Q1}$ .

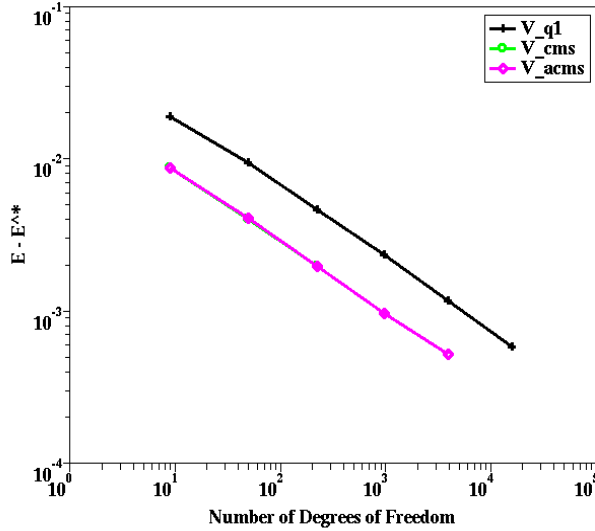


FIGURE 4. Comparison of special finite element methods for problem (46).

For the curves in Figure 4, the special basis functions  $z_{1,*}$ ,  $\varphi_P$ , and  $\psi_e$ , were approximated with  $16 \times 16$  bilinear finite elements in a square element of  $\mathcal{T}_n$ , *i.e.*  $h_f = h/16$ . Figure 5 illustrates the convergence of the energy  $\mathcal{E}$  for the subspace  $V_{ACMS}$  with a fixed mesh size  $h$  as  $m = h/h_f$  increases. A ratio of  $m = 16$  is sufficient

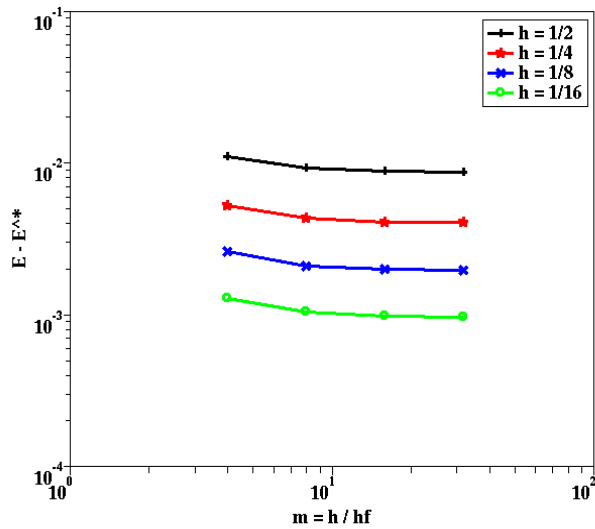


FIGURE 5. Effect of subcell mesh size to compute basis functions of  $V_{ACMS}$  for problem (46).

to compute numerically the special basis functions.

### 5.3. Experiments with a varying coefficient

Consider the problem

$$\begin{cases} -\nabla \cdot \left( \frac{1}{1.2 + \cos(32\pi x(1-x)y(1-y))} \nabla u(x,y) \right) = f & \text{on } \Omega \\ u = 0 & \text{in } \partial\Omega \end{cases} \quad (47)$$

We choose  $f(x,y) = 64\pi [x(1-x) + 2y(1-y)]$  such that the exact solution  $u$  is

$$u(x,y) = (1.2 \times 32\pi)x(1-x)y(1-y) + \sin(32\pi x(1-x)y(1-y)).$$

Note that the coefficient  $c$  oscillates while the source term  $f$  does not.

Introduce a mesh  $\mathcal{T}_n$  composed of squares with uniform mesh size  $h = 1/n$ .  $\mathcal{T}_n$  contains  $n^2$  elements,  $(n-1)^2$  interior points, and  $2n(n-1)$  interior edges.

#### 5.3.1. Convergence plots

We compare the accuracy of computed solutions using the finite-dimensional subspaces  $V_{Q1}$ ,  $V_{MsFEM-O}$ ,  $V_{ACMS}$ , and  $V_{CMS}$ . Since the coefficient  $c$  is varying, the subspace  $V_{MsFEM-O}$  is different from the subspace  $V_{Q1}$ .

Figure 6 plots convergence curves for the difference of energies, which is proportional to the energy norm of the error, in terms of the number of degrees of freedom. For this problem, the value for  $\mathcal{E}^*$  is

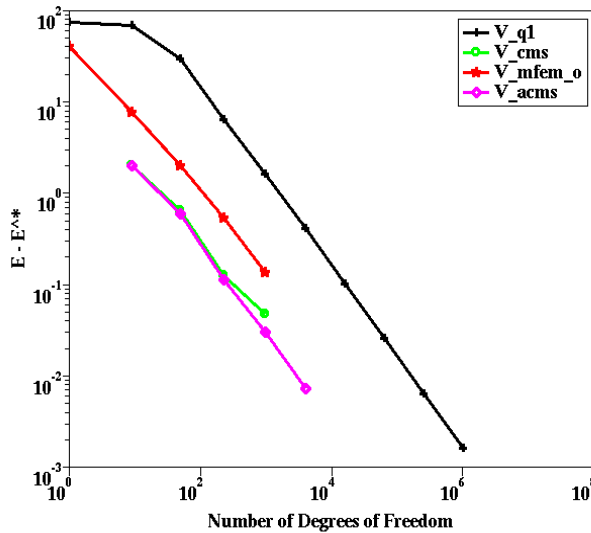


FIGURE 6. Comparison of special finite element methods for problem (47).

$$\mathcal{E}^* = -132.67094817007. \quad (48)$$

As expected, the bilinear finite element has a convergence rate proportional to  $h^2$  or inversely proportional to the total number of degrees of freedom. The curves for  $V_{CMS}$  and  $V_{ACMS}$  are aligned, indicating again that the local basis functions in  $V_{ACMS}$  approximate well the subspace spanned by the global eigenmodes for the

Schur and mass complements. For a fixed number of degrees of freedom, the approximate solutions computed in  $V_{CMs}$  and in  $V_{ACMs}$  are the most accurate followed by the subspace  $V_{MsFEM-O}$ . The approximate solution in  $V_{Q1}$  is the least accurate. The solution from  $V_{ACMs}$  is more accurate than the solution from  $V_{MsFEM-O}$ , highlighting the importance of the edge functions  $\psi_e$  and the fixed-interface modes  $z_{1,j}$ . To reach a fixed level of accuracy for this problem,

- $V_{MsFEM-O}$  requires 15 times less degrees of freedom than  $V_{Q1}$ ,
- $V_{ACMs}$  requires almost 55 times less degrees of freedom than  $V_{Q1}$ .

Table 2 compares the approximations obtained with the subspaces  $V_{Q1}$ ,  $V_{MsFEM-O}$ , and  $V_{ACMs}$ . For this

$h$	Matrix Dimension			Matrix Non-Zeros			$\mathcal{E} - \mathcal{E}^*$		
	$V_{Q1}$	$V_{MsFEM-O}$	$V_{ACMs}$	$V_{Q1}$	$V_{MsFEM-O}$	$V_{ACMs}$	$V_{Q1}$	$V_{MsFEM-O}$	$V_{ACMs}$
1/2	1	1	9	1	1	25	75.1	41.0	2.02
1/4	9	9	49	49	49	361	69.3	7.64	0.60
1/8	49	49	225	361	361	2,185	29.9	2.02	0.11
1/16	225	225	961	1,849	1,849	10,441	6.42	0.53	0.03
1/32	961	961	3,969	8,289	8,289	45,385	1.63	0.13	0.007

TABLE 2. Matrix dimension, matrix non-zeros, and energy error for different special finite element methods

example, the subspaces  $V_{MsFEM-O}$  and  $V_{ACMs}$  generate good approximations of  $u$  on meshes that are too coarse for  $V_{Q1}$  or the piecewise linear interpolation. The subspaces  $V_{Q1}$  and  $V_{MsFEM-O}$  generate matrices with the same dimensions, the same sparsity patterns, and an average of 9 non-zero entries per row. The subspace  $V_{ACMs}$  generates a matrix with an average of 12 non-zero entries per row. For  $h = 1/2$ , the subspace  $V_{ACMs}$  reaches a level of accuracy that the subspace  $V_{Q1}$  reaches when  $h$  is close to  $1/30$ . This ratio of 15 between the mesh sizes corresponds to a factor 55 for the degrees of freedom. Between  $V_{MsFEM-O}$  and  $V_{ACMs}$ , the subspace  $V_{ACMs}$  uses 4 times less degrees of freedom than  $V_{MsFEM-O}$  that would correspond to a ratio of 4 between the mesh sizes.

For the curves in Figure 6, the special basis functions were approximated with, at least,  $32 \times 32$  bilinear finite elements in any square element of  $\mathcal{T}_n$ , *i.e.*  $h_f \leq h/32$ . Figure 7 illustrates the convergence of the energy for the subspace  $V_{ACMs}$  with a fixed mesh size  $h$  as  $m = h/h_f$  increases. For this problem, a ratio of  $m = 32$  appears sufficient to compute numerically the special basis functions. Further analysis is required to define a priori rules for choosing  $m$ ; see, for instance Brezzi and Marini [7] for a study on two-level methods.

### 5.3.2. Impact of basis functions $\psi_e$ and $z_{1,*}$

The error bound (24) and the discussion at the end of section 2 highlight the importance of approximating the components of  $u$  in  $V_{\Omega_j}$  and in  $V_{\Gamma}$ . Failure to do so might require a finer partition  $\mathcal{T}$  and a larger number of degrees of freedom in order to reach a prescribed level of accuracy, as implied by the results of Table 2. In the next experiment, we emphasize the importance of the functions  $\varphi_P$ ,  $\psi_e$ , and  $z_{1,*}$ . We compute approximate solutions with the following finite-dimensional subspaces:

- $V_{MsFEM-O} = \text{span}(\varphi_P; \text{vertex } P \in \Omega)$ ;
- $V_{MsFEM-O-INT} = V_{MsFEM-O} \oplus \text{span}(z_{1,j}; 1 \leq j \leq J)$ ;
- $V_{MsFEM-O-EDGE} = V_{MsFEM-O} \oplus \text{span}(\psi_e; \text{edge } e \subset \Omega)$ ;
- $V_{ACMs} = V_{MsFEM-O} \oplus \text{span}(\psi_e; \text{edge } e \subset \Omega) \oplus \text{span}(z_{1,j}; 1 \leq j \leq J)$ .

Note that  $V_{MsFEM-O}$  and  $V_{MsFEM-O-EDGE}$  are proper subspaces of  $V_{\Gamma}$  while  $V_{MsFEM-O-INT}$  and  $V_{ACMs}$  have components in  $V_{\Omega_j}$  and  $V_{\Gamma}$ .

Figure 8 plots convergence curves for the energy difference in terms of the number of degrees of freedom. The curves for  $V_{MsFEM-O}$ , for  $V_{MsFEM-O-INT}$ , for  $V_{MsFEM-O-EDGE}$ , and for  $V_{ACMs}$  were computed on the same set of partitions. Recall that, on a given partition  $\mathcal{T}$ , all these subspaces have different dimension.

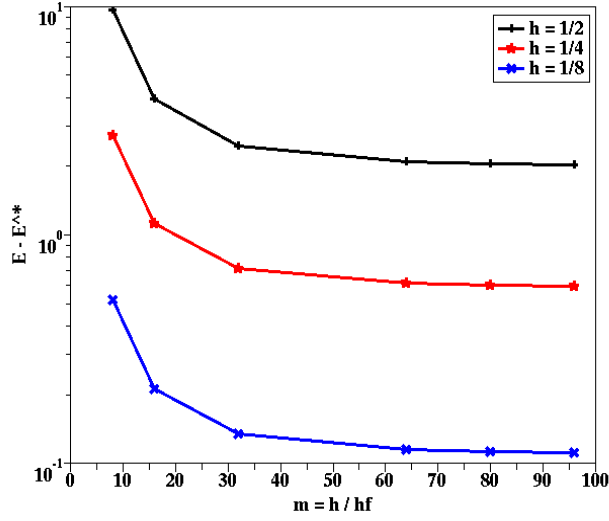


FIGURE 7. Effect of subcell mesh size to compute basis functions of  $V_{ACMS}$  for problem (47).

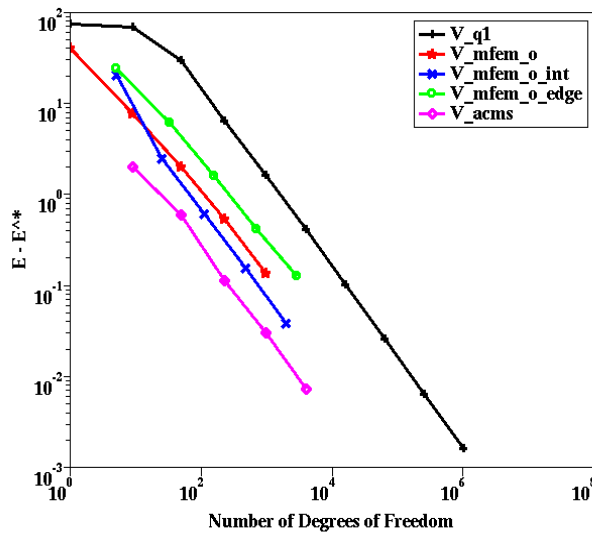


FIGURE 8. Comparison of subspaces motivated by the decomposition (11) for problem (47).

For a fixed level of accuracy, the approximate solution in  $V_{Q1}$  requires the largest number of degrees of freedom, followed by the approximation in  $V_{MsFEM-O-EDGE}$ , in  $V_{MsFEM-O}$ , in  $V_{MsFEM-O-INT}$ , and in  $V_{ACMS}$ . The subspaces  $V_{MsFEM-O}$  and  $V_{MsFEM-O-EDGE}$  approximate only the component of the solution  $u$  in  $V_{\Gamma}$ . Their respective convergence curves indicate that adding more basis functions in  $V_{\Gamma}$  does not improve the accuracy

per degree of freedom because these subspaces do not approximate the components in  $V_{\Omega_j}$ . On the other hand, adding the first fixed-interface eigenmodes to  $V_{MsFEM-O}$  improves the accuracy per degree of freedom. Indeed, the subspace  $V_{MsFEM-O-INT}$  approximates now all the components of  $u$ . Incorporating all the functions  $\phi_P$ ,  $\psi_e$ , and  $z_{1,j}$  in  $V_{ACMS}$  gives the best accuracy per degree of freedom among all the subspaces.

We emphasize that, on a given partition  $\mathcal{T}$ , the subspace  $V_{ACMS}$  is larger than  $V_{MsFEM-O}$  and computes a more accurate approximation to  $u$ . However, the gain in accuracy is so large that the accuracy with  $V_{MsFEM-O}$  on  $\mathcal{T}$  is reached with a subspace  $V_{ACMS}$  built on a partition coarser than  $\mathcal{T}$ . For this example, the subspace  $V_{ACMS}$  reaches the same level of accuracy than the subspace  $V_{MsFEM-O}$  with 4 times less degrees of freedom. This ratio of 4 in the number of degrees of freedom translates into a coarser partition with a mesh size smaller by a factor 4.

### 5.3.3. Impact of choice for the trace of $\varphi_P$

When building the approximating subspace  $V_{ACMS}$ , the definition of functions  $\varphi_P$  requires a choice of traces on  $\Gamma$ . Even though the functions  $\varphi_P$  still reside in  $V_\Gamma$ , different traces on  $\Gamma$  result in different approximating subspaces. For example, we could use the functions  $\varphi_P^L$  satisfying the boundary value problem (30) and having the same trace on  $\Gamma$  as the bilinear shape function  $N_P$  (the piecewise linear variation on  $\Gamma$  is indicated by the superscript  $L$ ). Figure 9 plots such a trace for  $\varphi_P^L$ .

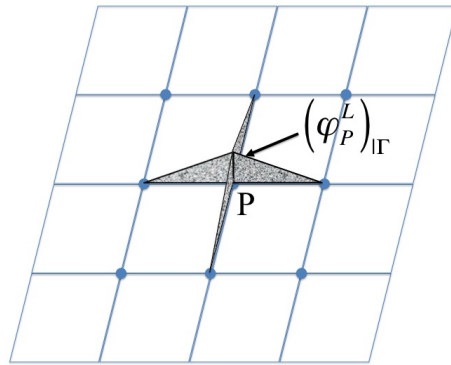


FIGURE 9. Trace of  $\varphi_P^L$  along  $\Gamma$  for a domain partitioned into 16 subdomains

Figure 10 plots convergence curves for the energy difference in terms of the number of degrees of freedom for solutions computed with the subspaces  $V_{ACMS}$  and  $V_{ACMS-L}$ . The subspace  $V_{ACMS-L}$  differs only from  $V_{ACMS}$  by the replacement of the functions  $\varphi_P$  with  $\varphi_P^L$ . Note that when  $c$  is constant, the subspaces  $V_{ACMS-L}$  and  $V_{ACMS}$  are equal. The approximation with  $V_{ACMS-L}$  appears to require a finer mesh to reach the asymptotic regime. Before reaching its asymptotic regime, the curve for  $V_{ACMS-L}$  exhibits a bump. The curves for  $V_{ACMS-L}$  and  $V_{ACMS}$  are different. But the curve for  $V_{ACMS-L}$  appears to reach asymptotically the curve for  $V_{ACMS}$ , which would be consistent with the case where  $c$  is constant.

This experiment highlights the importance of choosing an appropriate trace on  $\Gamma$  for the function  $\varphi_P$  in order to preserve the property that the subspace  $V_{ACMS}$  approximates well the subspace  $V_{CMS}$ .

## 5.4. Experiments with another varying coefficient

Finally, consider the problem

$$\begin{cases} -\nabla \cdot (c(\mathbf{x}) \nabla u(\mathbf{x})) = f(\mathbf{x}) & \text{on } \Omega, \\ u = 0 & \text{in } \partial\Omega. \end{cases} \quad (49)$$

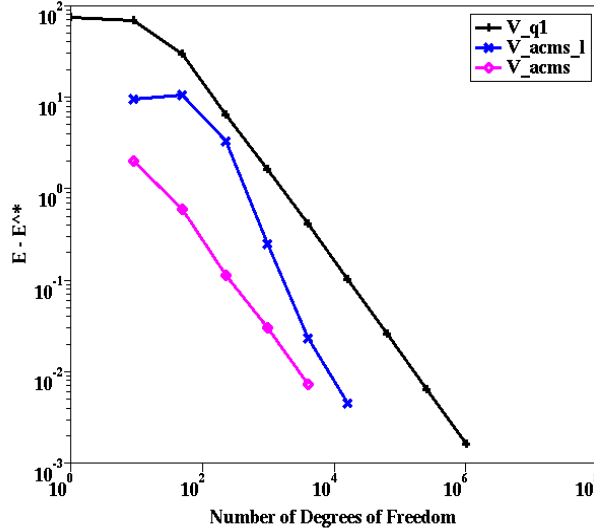


FIGURE 10. Comparison of two choices for the functions  $\varphi_P$  when solving problem (47).

We choose  $f = -1$  and the scalar coefficient  $c$

$$c(x, y) = \frac{2 + 1.8 \sin(25\pi x)}{2 + 1.8 \cos(25\pi y)} + \frac{2 + \sin(25\pi y)}{2 + 1.8 \sin(25\pi x)}. \quad (50)$$

This example was studied in the paper [11].

On a mesh  $\mathcal{T}_n$  made of squares with uniform mesh size  $h = 1/n$ , we compare the accuracy of computed solutions when using the finite-dimensional subspaces  $V_{Q1}$ ,  $V_{MsFEM-O}$ ,  $V_{ACMS}$ , and  $V_{CMS}$ . Figure 11 plots convergence curves for half the energy norm of the error in terms of the number of degrees of freedom. The reference energy  $\mathcal{E}^*$ ,

$$\mathcal{E}^* = -0.004717883361515083, \quad (51)$$

is computed by Richardson extrapolation based on energies computed with bi-quadratic finite elements and with quintic finite elements using COMSOL Multiphysics<sup>5</sup>.

All the methods have a convergence rate inversely proportional to the total number of degrees of freedom. For a fixed number of degrees of freedom, the approximate solution computed in  $V_{CMS}$  is the most accurate followed by the subspaces  $V_{ACMS}$  and  $V_{MsFEM-O}$ . The approximate solution in  $V_{Q1}$  is the least accurate. Here the curves for  $V_{CMS}$  and  $V_{ACMS}$  are different. The approximation with  $V_{ACMS}$  appears to require a finer mesh to reach the asymptotic regime. Before reaching its asymptotic regime, the curve for  $V_{ACMS}$  exhibits a bump. This bump seems similar to the one for  $V_{ACMS-L}$ , described in section 5.3.3. It was removed when the functions  $\varphi_P^L$  were replaced by the functions  $\varphi_P$ . This experiment suggests that, for this example, the current choice of trace on  $\Gamma$  for  $\varphi_P$  might not be optimal. Further analysis is required to find a different choice of trace functions that would allow  $V_{ACMS}$  to attain its asymptotic regime with fewer degrees of freedom.

<sup>5</sup>Version 3.5a, see [www.comsol.com](http://www.comsol.com)

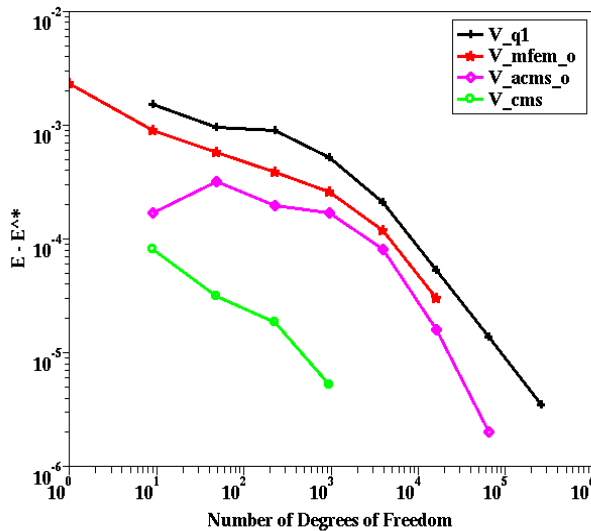


FIGURE 11. Comparison of special finite element methods for problem (49).

## 6. CONCLUSIONS

We have presented a new conforming special finite element method. The approach is based on the classical idea of component mode synthesis and exploits a  $H_0^1(\Omega)$  orthogonal decomposition. Fixed-interface eigenmodes, vertex-based harmonic extensions, and edge-based modes define the approximating subspace  $V_{ACMS}$ . We illustrated theoretically and numerically the importance of the three types of functions to obtain an accurate approximate solution. On academic examples, the new approximation subspace is, for the same number of degrees of freedom, more accurate than the bilinear finite element and the multiscale finite element method.

## ACKNOWLEDGEMENTS

The authors acknowledge the useful comments from the anonymous referees and Dan Segalman of Sandia National Laboratories. They also thank Prof. J. Osborn (U. Maryland) and Prof. U. Banerjee (Syracuse U.) for enlightening discussions about the generalized finite element method and the  $n$ -width.

U. L. Hetmaniuk was supported in part by the Laboratory Directed Research and Development program at Sandia National Laboratories.

R. B. Lehoucq was supported by the Laboratory Directed Research and Development program at Sandia National Laboratories. Sandia is a multiprogram laboratory operated by Sandia Corporation, a Lockheed Martin Company, for the U.S. Department of Energy under contract DE-AC04-94AL85000.

## REFERENCES

- [1] I. Babuška, U. Banerjee, and J. Osborn. On principles for the selection of shape functions for the generalized finite element method. *Comput. Methods Appl. Mech. Engrg.*, 191:5595–5629, 2002.
- [2] I. Babuška, U. Banerjee, and J. E. Osborn. Generalized finite element methods—main ideas, results and perspective. *Int. J. Comp. Meths.*, 1(1):67–103, 2004.
- [3] I. Babuška, G. Caloz, and J. Osborn. Special finite element methods for a class of second order elliptic problems with rough coefficients. *SIAM J. Numer. Anal.*, 31(4):945–981, 1994.

- [4] I. Babuška and J. E. Osborn. Generalized finite element methods: Their performance and their relation to mixed methods. *SIAM J. Numer. Anal.*, 20(3):510–536, 1983.
- [5] J. K. Bennighof and R. B. Lehoucq. An automated multilevel substructuring method for eigenspace computation in linear elastodynamics. *SIAM J. Sci. Comput.*, 25(6):2084–2106, 2004.
- [6] F. Bourquin. Component mode synthesis and eigenvalues of second order operators: Discretization and algorithm. *Mathematical Modelling and Numerical Analysis*, 26:385–423, 1992.
- [7] F. Brezzi and L. Marini. Augmented spaces, two-level methods, and stabilizing subgrids. *Int. J. Numer. Meth. Fluids*, 40:31–46, 2002.
- [8] R. R. Craig, Jr. and M. C. C. Bampton. Coupling of substructures for dynamic analysis. *AIAA Journal*, 6(7):1313–1319, 1968.
- [9] Y. Efendiev and T. Hou. *Multiscale Finite Element Methods: Theory and Applications*, volume 4 of *Surveys and Tutorials in the Applied Mathematical Sciences*. Springer New York, first edition, 2009.
- [10] U. Hetmaniuk and R. B. Lehoucq. Multilevel methods for eigenspace computations in structural dynamics. In *Domain Decomposition Methods in Science and Engineering*, volume 55 of *Lecture Notes in Computational Science and Engineering*, pages 103–114. Springer-Verlag, 2007.
- [11] T. Hou and X. Wu. A multiscale finite element method for elliptic problems in composite materials and porous media. *J. Comput. Phys.*, 134:169–189, 1997.
- [12] W. C. Hurty. Vibrations of structural systems by component-mode synthesis. *Journal of the Engineering Mechanics Division, ASCE*, 86:51–69, 1960.
- [13] J. Nolen, G. Papanicolaou, and O. Pironneau. A framework for adaptive multiscale methods for elliptic problems. *Multiscale Modeling & Simulation*, 7(1):171–196, 2008.
- [14] A. Quarteroni and A. Valli. *Domain Decomposition Methods for Partial Differential Equations*. Numerical Mathematics and Scientific Computation. Oxford University Press, Oxford, UK, first edition, 1999.